

## **General Disclaimer**

### **One or more of the Following Statements may affect this Document**

- This document has been reproduced from the best copy furnished by the organizational source. It is being released in the interest of making available as much information as possible.
- This document may contain data, which exceeds the sheet parameters. It was furnished in this condition by the organizational source and is the best copy available.
- This document may contain tone-on-tone or color graphs, charts and/or pictures, which have been reproduced in black and white.
- This document is paginated as submitted by the original source.
- Portions of this document are not fully legible due to the historical nature of some of the material. However, it is the best reproduction available from the original submission.

NASA Technical Memorandum 79133

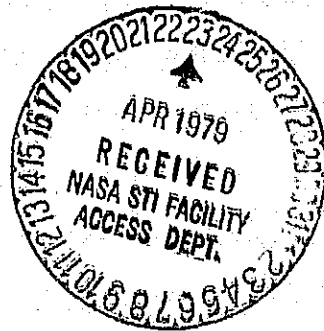
(NASA-TM-79133) ANALYSIS OF HIGH VELOCITY  
IMPACT ON HYBRID COMPOSITE FAN BLADES (NASA)  
17 p HC A02/MF A01 CSCL 21E

N79-20398

63  
03/39  
Unclas  
19839

ANALYSIS OF HIGH VELOCITY IMPACT  
ON HYBRID COMPOSITE FAN BLADES

C. C. Chamis and J. H. Sinclair  
Lewis Research Center  
Cleveland, Ohio



Prepared for the  
Twentieth Structures, Structural Dynamics and Materials Conference  
cosponsored by AIAA, ASME, ASCE, and AHS  
St. Louis, Missouri, April 4-6, 1979

# ANALYSIS OF HIGH VELOCITY IMPACT ON HYBRID COMPOSITE FAN BLADES

by C. C. Chamis and J. H. Sinclair

NASA Lewis Research Center  
Cleveland, Ohio

## INTRODUCTION

Application of advanced fiber composites to turbine engine fan blades offers several potential advantages. The most significant of these are: (1) elimination of the mid-span shroud which results in improved engine efficiency; (2) lighter engine and aircraft weights which result in reduced fuel consumption; and (3) higher possible tip speeds which can reduce the number of fan or compressor stages and result in fewer parts and lower initial and operating costs.

One major problem with the application of advanced fiber composites to fan blades has been their low resistance to impact, in general, and to bird ingestion and other foreign object damage (FOD) in particular. A major difficulty in predicting impact resistance of composite fan blades has been the limitations of available analysis methods in coping with the complex problem of predicting the local and global dynamic response when subjected to high-velocity impact. This paper describes recent developments in the analysis of high-velocity impact of composite blades using a computerized capability which is under development at the NASA Lewis Research Center.

Briefly, at the present stage of development, the method consists of coupling a composites mechanics computer code with the direct-time integration feature of NASTRAN. All aspects of composite mechanics from micromechanics, to laminate analysis and combined stress failure are handled via the composite mechanics computer code. The structural dynamics aspects of the high-velocity impact are handled via NASTRAN. The discussion of the application of the computerized method in this paper is limited to the linear dynamic response of an interply hybrid composite fan blade subjected to a high-velocity impact of a two pound bird.

## BLADE GEOMETRY, HYBRID COMPOSITE AND FINITE ELEMENT MODEL

A photograph of the blade investigated is shown in figure 1. The blade was designed and made by the General Electric Company (ref. 1). The nominal dimensions of the blade are 21 inches long, and 12 inches wide at the tip. The thickness varied along the blade centerline from about 0.90 inches at the root of 0.30 inches at the tip. The nominal leading and trailing edge thicknesses were 0.13 inches. The angle of twist was approximately  $33^\circ$ . The nominal tip radius from the center of the shaft was about 35 inches.

The interply hybrid composite blade consisted of boron/epoxy outer plies at  $\pm 45^\circ$  (measured from the radial line), S-glass/epoxy plies at  $0^\circ$  and at  $\pm 45^\circ$  near the root, s-glass cloth filler plies at the root, and kevlar 49/epoxy plies at  $0^\circ$ ,  $\pm 45^\circ$  and  $90^\circ$  interspersed through the thickness of the blade. The blade also had metallic leading edge protection. The total number of different materials in the hybrid composite blade was five. The nominal ply thickness was 0.010 inches. The fiber volume ratio was about 0.60. The several  $0^\circ$  and  $\pm 45^\circ$  S-glass/epoxy plies near the root were added to increase bending strength of the blade for improved impact resistance.

The blade was modeled using 127 nodes (grid points) and 210 anisotropic-material, triangular plate elements (CTR1A2 in the NASTRAN (ref. 2) element library). Each element had different material properties (fig. 2).

## ANALYSIS, RESULTS AND DISCUSSION

The high velocity impact analysis of the hybrid composite blade was performed using the computerized capability depicted schematically in figure 3. This computerized capability consists of two major modules: NASTRAN (ref. 2) and composite mechanics (ref. 3) which communicate with each other via a pre and a post processor. Parts of this computerized capability have been used extensively for the analysis of composite blades (refs. 4 to 6).

### Input Data

The input data for the blade was supplied for four span sections: bottom of root, beginning of airfoil, midspan of airfoil, and tip. The remaining blade geometry, grid (nodal) point coordinates of grid point, thickness, and element connection cards were generated by the preprocessor. The number of plies at each grid point, ply stacking sequence, and ply type were also generated by the preprocessor. The ply properties were generated by the composite micromechanics available in the composite mechanics module which accesses a computer resident composite material properties data bank via the preprocessor. The ply properties, stacking sequence, composite system, and number of plies (including the metallic leading edge) were used in the laminate analysis (available in the composite mechanics module) to generate the laminate properties at each grid point. The laminate properties at each grid point were then used in the preprocessor to generate the properties (MAT2 and PTR1A2) for each element (210 elements, fig. 2). The information in each MAT2 card consisted of four stress-strain coefficients, density and three thermal expansion coefficients.

The boundary conditions simulating blade attachment consisted of fixing the x and z displacement of grid points 123-127, figure 2, the y displacement in grid point 125, and the three rotations of grid points 123-127. In addition, the global z-rotation was constrained in grid points 109 to 127 (fig. 2). These boundary conditions were entered manually in the NASTRAN bulk data via single point constraint (SPC) cards. The rotation speed, the forcing function simulating the bird impact, and the impact region (to be described later) were entered manually using the appropriate NASTRAN bulk data cards.

### Vibration Frequencies

In order to confirm that the interply hybrid composite blade was properly modeled, the first five cantilever vibration frequencies were computed and compared with available measured data. The results are summarized in table 1. As can be seen the

predicted results are within 7 percent of the measured data. This agreement is considered to be excellent in view of the fact that the hybrid composite blade consists of five different materials varying in amount and direction at each grid point.

The vibration mode shape associated with the fifth (5) vibration frequency shown in figure 4 is of interest because most of the activity of this mode shape is near the leading edge tip which is the vicinity of the impact. The two nodal lines could provide fracture paths. This of course would depend on the vibration mode and amplitude at the instant of impact.

#### Steady State Loads

The hybrid composite blade was also analyzed by considering the steady state loads acting on the blade. The steady state loads consist of the aerodynamic pressures and temperatures and centrifugal loads due to the rotation of the blade in general. Previous studies (ref. 5) have shown, however, that the aerodynamic loads (pressures and temperatures) produce negligible stresses (less than 5 percent) in the blade compared to the stresses produced by the centrifugal loads. The stresses due to centrifugal loads were determined using the shaft rotational speed of 3157 revolutions per minute (RPM). The calculated composite average stresses in the radial direction were less than 10 ksi in the airfoil. The stress was 12 ksi at the transition region from the airfoil to the root near the trailing edge (fig. 2), and 10 ksi at the point of blade maximum thickness, near the blade mid-chord. These calculated stresses were within about 11 percent of those determined from strain gage data (respectively, 13.5 and 9 ksi) in the work performed in reference 1. An agreement within 11 percent between calculated and predicted composite stress is considered very good since the blade is made from four different composite materials and a metallic leading edge protection device and that the number of plies are different at each grid point as was mentioned previously.

The vibration frequencies and centrifugal stress comparisons provide confidence that hybrid composite blades with complex geometries and made from several ma-

materials can be modeled adequately using the computerized capability depicted schematically in figure 3. It is reasonable to conclude, then, that this computerized capability will describe the response of hybrid composite blades with reasonable accuracy and of composite blades in general, subjected to high velocity impact prior to the onset of local damage anywhere in the blade.

#### High Velocity Impact

The analysis for the high velocity impact was performed using the direct time integration capability of NASTRAN (Rigid FORMAT 9). Briefly, the structural dynamic response of the blade is determined by solving the following equation

$$[M] \{\ddot{u}\} + [C] \{\dot{u}\} + [K] \{u\} = \{F(t)\} \quad (1)$$

The notation in equation (1) is as follows:  $[M]$  is the global mass matrix;  $\{u\}$ ,  $\{\dot{u}\}$  and  $\{\ddot{u}\}$  are the grid points displacement vector, grid points velocity vector and grid points acceleration vector, respectively;  $[C]$  is the global structural and material damping matrix;  $[K]$  is the global stiffness matrix; and  $\{F(t)\}$  is the impact force vector.

The impact force vector used in the analysis was provided by the contractor (ref. 1) and is shown in figure 5. It peaks at about 15 000 pounds and acts on the blade (contact time) for approximately 0.5 milli-seconds (MSEC). The impact conditions represented by this force vector are as follows: (1) rotor speed, 3157 RPM; (2) incidence angle,  $33^\circ$ ; (3) impact location 80 percent of span, approximately 32 inch radius; (4) bird relative velocity, 927 feet per second (FT/SEC); (4) bird weight, 2 pounds; and (6) bird slice, 8 ounces. . The impact force vector (fig. 5) was assumed to act on the blade along the grid point line containing nodes 19 to 27 (fig. 2) for analysis purposes.

The global mass  $[M]$  and stiffness  $[K]$  matrices were generated by NASTRAN using the information from the input data described previously. The damping matrix  $[C]$  was generated by NASTRAN using a damping factor of 0.005 and the first vibration frequency (with geometric stiffening) of 74 cycles per second (CPS).

Typical transient results obtained from this analysis for blade tip displacement and velocity, reaction force, and composite stresses at the impact point are described below.

The z-component of the leading edge tip displacement versus time in milliseconds (MSEC) is shown in figure 6. The contact time and estimated maximum tip displacements from high-speed movies are also shown in this figure. The interesting points to be noted in figure 6 are: (1) the predicted displacement peaks shortly after the impact time; (2) the predicted displacement remains between about 4 and 7 inches for approximately 3 MSEC which corresponds to about 6 times the contact time and (3) the predicted displacement reaches the magnitude range which was estimated from high-speed movies taken during impact. The estimated vibration frequency from the first half wave is about 750 CPS which is close to the sixth vibration frequency (700 CPS) and indicates that the blade tip modes dominate at early times of impact, figure 4.

The velocity at the corresponding point is plotted versus time in figure 7. As can be seen, the velocity rises monotonically during the duration of contact and peaks at the end of the contact time reaching a magnitude of about 1500 feet per second. This peak velocity is about 1.5 times the blade tip rotational speed which is about 960 feet/sec (3157 RPM, 35 in. tip radius). The estimated frequency based on one-half wave length (from peak to valley) is about 880 CPS. This frequency is higher than that determined from the first half wave of the tip displacement, is close to the seventh vibration frequency of the blade (835 CPS), and substantiates further that the blade tip modes dominate at early times of impact.

The z-component of the reaction force at the root of the blade near the mid chord is plotted versus time in figure 8. This component reaches a magnitude of about -2500 pounds at the end of the contact time. Thereafter it changes directions and begins to oscillate, peaking at about 17 000 pounds at about 2.4 MSEC or about 5 times the contact time. The estimated vibration frequency from the first half wave is about



830 CPS. This frequency is between those obtained from the displacement and the velocity and almost coincides with the seventh vibration frequency of the blade (835 CPS). The following important point can be made in view of the plot in figure 8. Since the reaction force peaks beyond the contact time, blade root failures may occur at about twice the contact time or greater. In order for root failures to occur, the blade must be able to transmit the major part of the impact force to the root. In blades where the impact load causes extensive local damage, the peak reaction force at the root can be relatively small compared to the case with little or no local damage. Therefore, test conditions to demonstrate the impact resistance of composite blades must be selected with care since local damage and root failure occur at considerably different times.

Bending stresses on the suction surface at a point near the impact area are plotted versus time (assuming linear behavior and no fracture) in figure 9. The corresponding estimated strengths are also shown in the figure as straight lines parallel to the time axis. The most significant point to note in this figure is that the composite bending stresses reach their corresponding estimated strengths between about one-fourth and two-thirds of the contact time. This means that the impact conditions considered for this analysis will cause substantial local damage, and probably fracture, at very early times of the impact event. One logical conclusion is that the hybrid composite blade considered will not survive locally the imposed impact conditions. This conclusion is consistent with the local damage results (ref. 1).

Local fractures at early times will tend to decrease both the forcing function magnitude and the contact time. Both of these will decrease the impact reaction force at the root as well as the stresses in the root region. The net result is that the imposed impact conditions may not cause blade root failure during test. However, this does not imply that the blade root design may be adequate for the imposed impact conditions.

If it is assumed that no local fracture occurs at all, then, it can be seen in figure 9 that: (1) the chordwise stress peaks at about 310 ksi at the end of the contact time; (2) the spanwise stress peaks at about -110 ksi about 0.8 times the contact time; and (3) the in-plane shear peaks at about -153 ksi at about 1.5 times the contact time. Needless to say both the chordwise and the in-plane shear peak stresses are very high and will cause damage in any material. If no local failure occurs, the stresses at the base of the airfoil (grids 109 to 115, fig. 2) peak at about 2.0 times the contact time. In this region also the chordwise and inplane shear composite stresses are higher than the corresponding estimated strengths. At midchord for example, the peak chordwise stress is 90 ksi (compared to an estimated strength of 45 ksi) and the in-plane shear is 44 ksi (compared to 25 ksi). The spanwise composite stress, on the other hand, is about 80 ksi (compared to 90 ksi). A logical conclusion from the previous discussion is that the imposed impact conditions would probably cause root failures in the hybrid composite blade considered if no local failure occurs at the impact region.

It is noted that once damage has occurred, then, some kind of nonlinear analysis is needed in order to determine the subsequent dynamic response of the hybrid composite blade. The discussion of such an analysis is beyond the objective of this paper.

### SUMMARY OF RESULTS

The significant results of an investigation to perform an analysis of a hybrid composite blade subjected to high-velocity impact are as follows:

1. A computerized analysis capability was used which couples NASTRAN with a composite mechanics code to predict the dynamic response of hybrid composite blades prior to initial damage.
2. Predicted results from this capability for vibration frequencies and stresses were in good agreement with measured data.

3. Predicted tip displacements due to impact are in agreement with those magnitudes observed in high speed movies of the impact event.

4. The dynamic response (displacements, velocities and reaction forces) of the hybrid composite blade indicate that the high velocity impact excites the higher (mostly tip) vibration modes of the blade.

5. The predicted stresses reach magnitudes comparable to the corresponding composite strength at early times during the impact event.

6. The impact conditions considered in this investigation are sufficiently severe to cause both local damage at early impact times (fraction of the contact time) as well as root failure at later times.

#### REFERENCES

1. Oler, T. L.: Fiber Composite Fan Blade Impact Improvement Program, Final Report. Work Performed under contract by General Electric Co. NASA CR-135078, 1976.
2. McCormic, C. W.: NASTRAN User's Manual (Level 15). NASA SP 222(01), 1972.
3. Chamis, C. C.: Computer Code for the Analysis of Multilayered Fiber Composites-User's Manual. NASA TN D 7013, 1971.
4. Chamis, C. C. and Lynch, J. E.: High-Tip-Speed Fiber Composite Compressor Blades: Vibration and Strength Analysis. NASA TM X-71589, 1974.
5. Chamis, C. C. and Minich, M. D.: Structural Response of Fiber Composite Fan Blades. ASME Publication 75-GT-78, 1975. Also NASA TM X-71623, 1975.
6. Chamis, C. C.: Vibration Characteristics of Composite Fan Blades and Comparison with Measured Data. Journal of Aircraft, Vol. 14, No. 7, July 1977, pp. 664-647. Also NASA TM X-71893, 1976.

TABLE 1. - VIBRATION FREQUENCIES (CPS) OF  
A HYBRID COMPOSITE FAN BLADE

Mode	Measured*	Predicted	<u>Predicted</u> Measured
1	62	64	1.03
2	190	186	.98
3	288	303	1.05
4	425	454	1.07
5	667	653	.98

\*Reference 1.

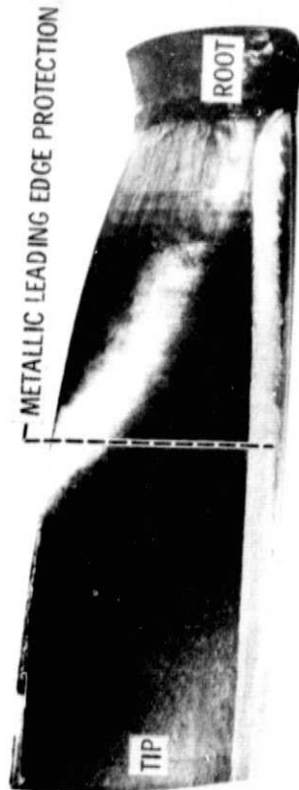


Figure 1. - Hybrid composite fan blade (nominal dimensions: 21 inches long, 12 inches wide at tip).

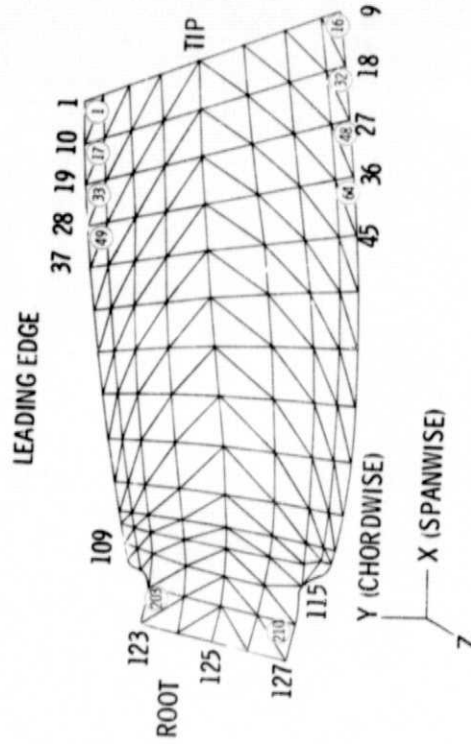


Figure 2. - Hybrid composite fan blade finite element representation schematic (127-nodes; 210-elements, 210-material properties).

ORIGINAL PAGE IS  
OF POOR QUALITY.

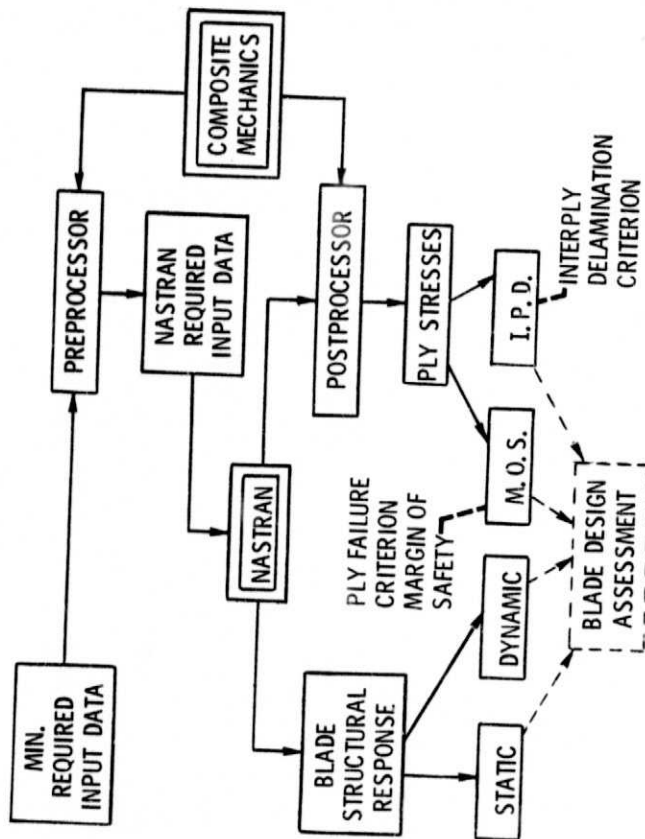


Figure 3. - Computerized capability for composite blade high-velocity impact analysis (NASTRAN coupled with composite mechanics).

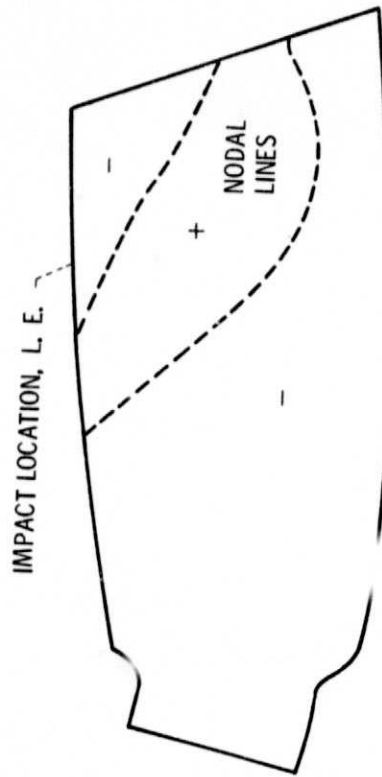


Figure 4. - Vibration mode shape 5 ( $f = 653$  CPS) of a hybrid composite fan blade.

ORIGINAL PAGE IS  
OF POOR QUALITY

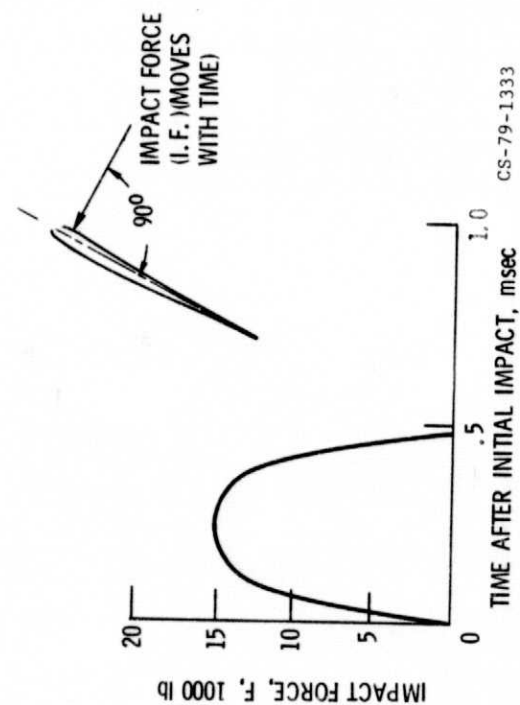


Figure 5. - Estimated impact force on a hybrid composite fan blade (80% span, 2-lb bird, takeoff power).

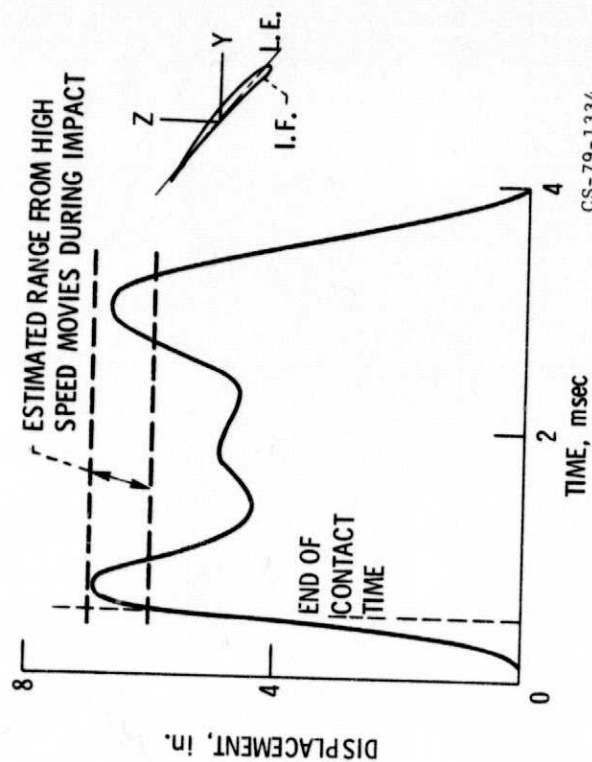


Figure 6. - Z-component of L.E. tip displacement of a hybrid composite fan blade, 2-lb bird impact.

CS-79-1334

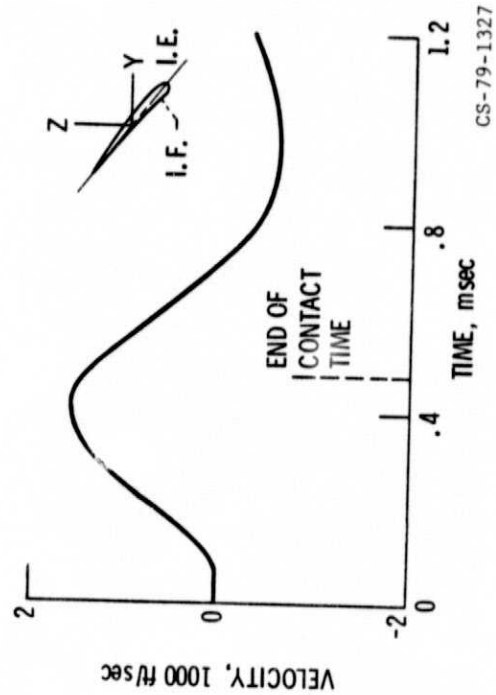


Figure 7. - Z-component of L.E. tip velocity of a hybrid composite fan blade, 2-lb bird impact.

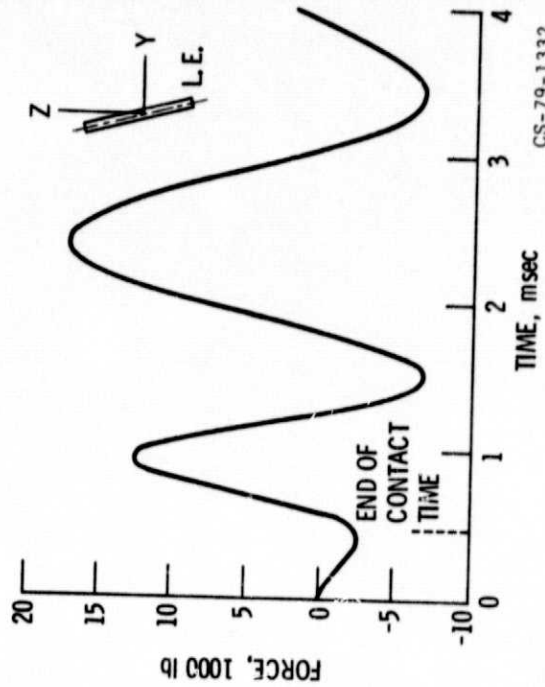


Figure 8. - Z-component of impact reaction force at root center of a hybrid composite fan blade.

ORIGINAL PAGE IS  
OF POOR QUALITY



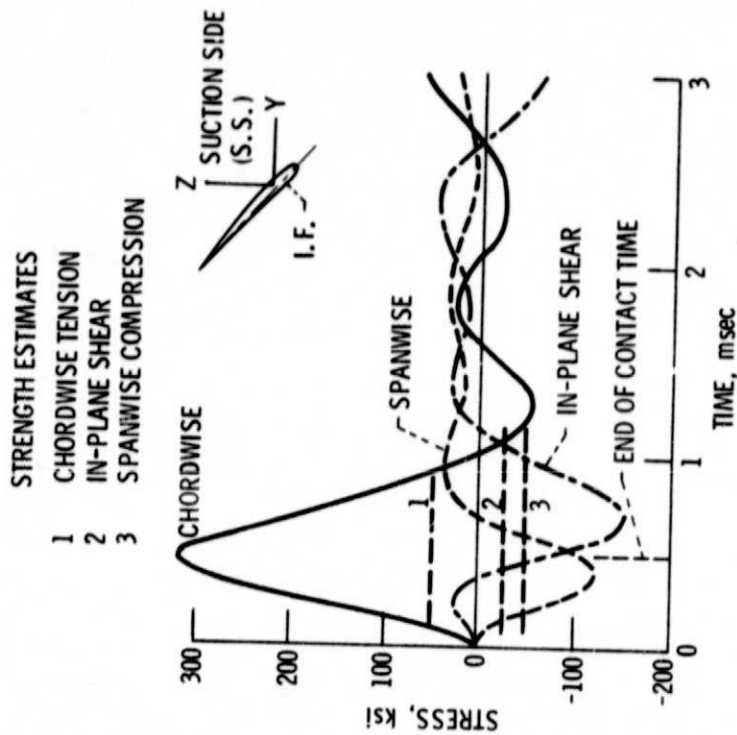


Figure 9. - Composite bending stresses near impact point (s.s.) of a hybrid composite fan blade, 2-lb bird impact.

1. Report No. NASA TM-70133		2. Government Accession No.		3. Recipient's Catalog No.	
4. Title and Subtitle ANALYSIS OF HIGH VELOCITY IMPACT ON HYBRID COMPOSITE FAN BLADES				5. Report Date	
				6. Performing Organization Code	
7. Author(s) C. C. Chamis and J. H. Sinclair				8. Performing Organization Report No. E-9979	
9. Performing Organization Name and Address National Aeronautics and Space Administration Lewis Research Center Cleveland, Ohio 44135				10. Work Unit No.	
				11. Contract or Grant No.	
12. Sponsoring Agency Name and Address National Aeronautics and Space Administration Washington, D.C. 20546				13. Type of Report and Period Covered Technical Memorandum	
				14. Sponsoring Agency Code	
15. Supplementary Notes					
16. Abstract <p>This paper describes recent developments in the analysis of high velocity impact of composite blades using a computerized capability which consists of coupling a composites mechanics code with the direct-time integration features of NASTRAN. The application of the capability to determine the linear dynamic response of an interply hybrid composite aircraft engine fan blade is described in detail. The predicted results agree with measured data. The results also show that the impact stresses reach sufficiently high magnitudes to cause failures in the impact region at early times of the impact event.</p>					
17. Key Words (Suggested by Author(s)) High velocity impact; Structural dynamics; Composite mechanics; NASTRAN; Interply hybrid composite; Composite fan blade; Bird impact; Vibration modes; Displacements; Velocities; Stresses				18. Distribution Statement Unclassified - unlimited STAR Category 39	
19. Security Classif. (of this report) Unclassified		20. Security Classif. (of this page) Unclassified		21. No. of Pages	
				22. Price*	